International Journal of Robotics and Control Systems
Vol. 5, No. 2, 2025, pp. 1278-1296
ISSN 2775-2658
http://pubs2.ascee.org/index.php/ijrcs

Active Disturbance Rejection Control for Unmanned Aerial Vehicle

Hakam Marwan [a,b,1,*], Amjad J. Humaidi [a,2], Huthaifa Al-Khazraji [a,3]

[a] Department of Control and System Engineering, University of Technology, Baghdad, 10069, Iraq
[b] College of Electronics Engineering, Nineveh University, Mosul, 41002, Iraq
[1] cse.23.15@grad.uotechnology.edu.iq; [2] amjad.j.humaidi@uotechnology.edu.iq; [3] 60141@uotechnology.edu.iq
* Corresponding Author

ARTICLE INFO

Article history
Received March 13, 2025
Revised April 04, 2025
Accepted May 12, 2025

Keywords
Tail-Sitter VTOL Aircraft;
Active Disturbance Rejection Control;
Extended State Observer;
Parameter Uncertainty

ABSTRACT

This paper presents the design and analysis of a roll motion control system for a vertical take-off and landing of unmanned aerial car (VTOL-UAV) during the hovering flight phase. Ensuring stability and disturbance rejection during hovering is a significant challenge for UAVs, as external disturbances can lead to instability. To address these challenges, this study proposes an Active Disturbance Rejection Control (ADRC) strategy to enhance the system's roll stability and disturbance rejection. The primary contribution is the development of an improved ADRC system by integrating different types of extended state observers (ESO) with a Nonlinear-Proportional-Derivative (NPD) controller. The paper evaluates three ESO types—Linear (LESO), Nonlinear (NESO), and Fractional Order (FOESO)—for system state estimation and disturbance compensation. By combining the best ESO with NPD controller, an enhanced ADRC system is formed and its performance is compared against a conventional Proportional-Integral-Derivative (PID) controller. Numerical simulations performed using MATLAB demonstrate that ADRC significantly improves roll stability and disturbance rejection under both disturbed and undisturbed conditions. The results indicate that the LESO provides the best estimation accuracy, leading to superior system robustness. The ADRC system with LESO outperforms the PID controller in all test cases, particularly in disturbance rejection and stability. The study concludes that ADRC with LESO is an effective solution for improving VTOL-UAV roll motion control during hovering providing a promising approach for future UAV applications in dynamic environments.

1. Introduction

Unmanned Aerial Vehicles (UAVs), often known as drones, have garnered considerable interest in recent years from a growing number of academics and engineers across diverse academic and scientific fields [1]-[6]. UAVs have historically been employed for military programs to carry out a comprehensive array of army activities [7]-[8]. However, significant advancements in the design and production of low-cost, highly reliable unmanned aerial vehicles, coupled with growing demand for their commercial deployment, have led to the widespread adoption of UAVs across a diverse range of civil and industrial applications [1]. In addition, UAVs' unique attributes, together with ease of use, speedy deployment to some distance-flung regions, high-

mobility, maneuverability, and their ability to hover, make them super applicants for civil and industrial programs [1]. Examples of such applications include search and rescue missions [9]-[12], precision agriculture monitoring [13], natural disaster and environmental monitoring [14]-[15], delivery of goods [16]-[19], and remote sensing [20]-[21]. An unmarried UAV (more than one UAV) may be used as communication relays or maybe aerial base stations (BSs) to provide wi-fi network insurance [22]-[24]. Applications for the Internet of Things (IoT) can also make use of UAVs. [25]-[28]. Physical items (also known as "matters") in such packages might not be capable of speak over an extended variety. In IoT packages, UAVs can then be utilized as dynamic gateways to transmit wireless information [29]-[30].

This paragraph discusses the importance of Active Disturbance Rejection Control (ADRC). The ADRC represents a paradigm shift in feedback control system design, offering a robust alternative to conventional PID and model-based approaches [31]-[36]. ADRC addresses the limitations of model dependency and tuning challenges by actively estimating and compensating for unknown dynamics and disturbances in real-time [37]. This technique demonstrates high robustness, maintaining consistent performance and stability margins despite significant plant parameter variations [38]. ADRC has proven effective in various applications, including active vibration control of seismically excited building structures [39]. Its key advantages include reduced sensitivity to input disturbances, simplified implementation, and the ability to function without precise system parameters [38]-[39]. ADRC comprises three key components: the tracking differentiator, the extended state observer (ESO), and nonlinear PID [40].

In the literature, many researchers have used different structures of controls a tail-sitter VTOL UAV system including the PID regulator [41], the model predictive controller [42], sliding mode control [43], disturbance observer-bases controller using H-infinity synthesis [43], active disturbance rejection control (ADRC) for attitude controller [44], and nonlinear robust controller [45]. As in step with past studies, a tail-sitter VTOL aircraft exhibits an herbal volatile conduct in vertical flight. Also, all through hover mode, tail-sitters have complex flight dynamics due to system uncertainties and outside disturbances. In [46], proposed a sliding mode control strategy using a high-gain observer for VTOL aircraft trajectory tracking. In [47], a control layout based on linear saturation features and the Lyapunov technique for manoeuvre in transition for tail-sitter drone.

This study highlights the developing of an Active Disturbance Rejection Control (ADRC) due to its potential to address machine uncertainties and outside disturbances without requiring a correct mathematical model. The core of ADRC is the Extended State Observer (ESO), which estimates and compensates for disturbances in real-time. However, specific ESO systems, together with linear, nonlinear, and fractional order, exhibit various levels of performance in disturbance rejection. The objective of this research is to analyze and compare the effectiveness of three types of ESO in ADRC structures. In addition, The ADRC is integrated with Nonlinear Proportional-Derivative (NPD) and the proposed ADRC-NPD method is compared with traditional PID. This examine affords treasured insights into the most appropriate selection of the feedback controller and demonstrates a sophisticated method for improving ADRC performance. The key contributions of this study may be summarized as follows:

- Development of an Enhanced ADRC Framework – This observe gives an progressed Active Disturbance Rejection Control (ADRC) strategy via integrating one of a kind styles of Extended State Observers (ESO) to beautify roll balance and disturbance rejection for VTOL-UAVs.
- Comparative Analysis of ESO Variants – The studies evaluate the overall performance of Linear (LESO), Nonlinear (NESO), and Fractional (FESO) Extended State Observers in estimating system states and compensating for outside disturbances.
- Integration of Nonlinear Proportional-Derivative (NPD) Control – A novel method is brought by using incorporating NPD manage inside the ADRC framework, and its effectiveness is as compared with the traditional PID controller.

- Numerical Validation via MATLAB Simulations – The proposed manipulate structures are tested through numerical simulations, demonstrating superior overall performance in disturbance rejection and roll balance below unique working conditions.

This is how the rest of the paper is structured: Section 2 provides a description of the Tail-Sitter VTOL Aircraft. Section 3 presents the design ADRC and PID controllers, Section 4 presents simulation results in MATLAB, and Section 5 concludes the study.

2. Dynamic Model of Tail-Sitter VTOL Aircraft

This section discusses the dynamic model of the Tail-Sitter VTOL aircraft. Before calculating the dynamic equations, the following assumptions are made:

1. The use of the Flat-Earth model equations is justified by the first assumption: The aircraft operates within a small local area [48].
2. The second assumption: The masses of the elevators and propeller blades are not taken into account [49].

Two coordinate frames are considered in light of Fig. 1:

- The first frame is the body-fixed frame (b-frame), which is attached to the aircraft and represented by (X, Y, Z).
- The second frame is the inertial reference frame, which follows the North-East-Down (NED) coordinate system and is represented by (x, y, z).

As demonstrated in [46], the kinematic equations for position, forces, and moments are derived from the configuration shown in Fig. 1.

$$\dot{p} = R(e)V \tag{1}$$

$$\dot{\Theta} = H(e)\Omega \tag{2}$$

$$m\dot{V} = -\Omega \times V + F \tag{3}$$

$$J\dot{\Omega} = -\Omega \times J.\Omega + \tau \tag{4}$$

The matrix $R(e)$ represents the transformation from the airframe to the fixed inertial coordinate system and is defined as follows:

$$\begin{bmatrix} C_\theta C_\psi & S_\phi S_\theta C_\psi - C_\phi S_\psi & C_\phi C_\theta C_\psi + S_\phi S_\psi \\ C_\theta S_\psi & S_\phi S_\theta S_\psi + C_\phi C_\psi & C_\phi S_\theta S_\psi - S_\phi C_\psi \\ -S_\theta & C_\theta S_\phi & C_\theta C_\phi \end{bmatrix} \tag{5}$$

- Sa = sin(a), Ca = cos(a)
- $p = [p_n p_e p_d]^T$ represents the position of the center of mass of the rigid body relative to the n-frame.
- $e = [e_0 \quad e_1 \quad e_2 \; e_3]^T$ symbolizes the current attitude's quaternion and is described as follows: $e = e_o + e_1 i + e_2 j + e_3 k$,
- $\Theta = [\phi\theta\psi]^T$ represents the orientation of the VTOL aircraft in the n-frame.
- The angular velocity produced by a series of Euler rotations from the body to the local reference system during hover flight is represented by the transformation matrix H(e).

Where t_θ denotes tan(θ), and the roll, pitch, and yaw angles, which are frequently utilized in aerodynamic applications, are defined by the Euler angles.

$$H(e) = \begin{bmatrix} 1 & t_\theta S_\phi & t_\theta C_\phi \\ 0 & C_\phi & -S_\phi \\ 0 & S_\phi/C_\theta & C_\phi/C_\theta \end{bmatrix} \quad (6)$$

F is the vector of external thrusts applied to the mass center of the VTOL aircraft, and the torque vector $\tau = [\tau_l \quad \tau_m \quad \tau_n]^T$ combines the torque components applied to the mass center of the VTOL aircraft in the body frame. The angular velocity in the body-fixed frame (b-frame) is represented by the vector $\Omega = [PQR]^T$. The flying aircraft's inertia matrix, J, can be represented by:

$$J = \begin{bmatrix} J_x & J_{xy} & J_{xz} \\ J_{yx} & J_y & J_{yz} \\ J_{zx} & J_{zy} & J_z \end{bmatrix} \quad (7)$$

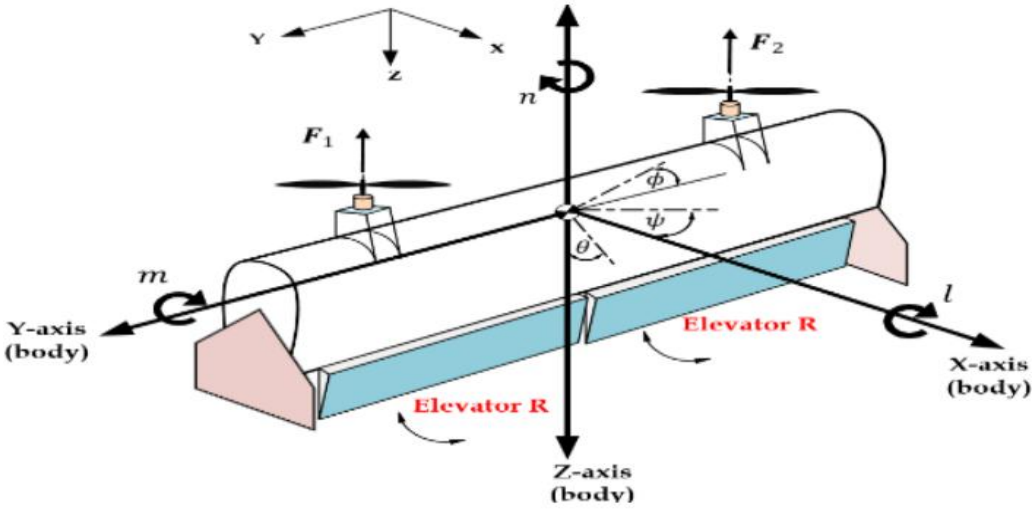

Fig. 1. Flight dynamics of tail-sitter vertical takeoff and landing aircraft [50]

If it is assumed that the xz-plane of the body-fixed frame in the Tail-Sitter VTOL aircraft configuration coincides with the plane of symmetry, the products of inertia J_{xy} and J_{yz}become negligible. Additionally, due to the symmetry of the Tail-Sitter configuration in the yz-plane, the product of inertia $J_{xz}$is also zero. Consequently, the inertia matrix and its inverse are expressed as follows.

$$J = \begin{bmatrix} J_x & 0 & 0 \\ 0 & J_y & 0 \\ 0 & 0 & J_z \end{bmatrix}, J^{-1} = \begin{bmatrix} 1/J_x & 0 & 0 \\ 0 & 1/J_y & 0 \\ 0 & 0 & 1/J_z \end{bmatrix} \quad (8)$$

The transformation matrix H, as defined in Equation (2), converts the angular velocity components resulting from Euler rotations from the body-fixed frame to the inertial reference frame, expressed as follows:

$$H(e) = \begin{bmatrix} 1 & \tan(\theta)\sin(\phi) & \tan(\theta)\cos(\phi) \\ 0 & \cos(\phi) & -\sin(\phi) \\ 0 & \sin(\phi)/\cos(\theta) & \cos(\phi)/\cos(\theta) \end{bmatrix} \quad (9)$$

Consequently, the kinematic Equation (2) can be expressed as follows:

$$\dot{\phi} = P + \tan\theta(Q\sin(\theta) + R\cos\phi) \quad (10)$$

$$\dot{\theta} = Q\cos\phi - R\sin\phi \quad (11)$$

$$\dot{\psi} = (Q\sin\ \phi + R\cos\ \phi)/\cos\ \theta \tag{12}$$

Utilizing the inertia matrix presented in Equation (6) with the thrust moments T_l, T_m and T_n as indicated in Fig. 1, Equation (4) can be rewritten by:

$$\dot{P} = (J_y - J_z)QR/J_x + T_l/J_x \tag{13}$$

$$\dot{Q} = (J_z - J_x)PR/J_y + T_m/J_y \tag{14}$$

$$\dot{R} = (J_x - J_y)PQ/J_z + T_n/J_z \tag{15}$$

To derive the roll dynamics, it is assumed that the yaw and pitch rates are zero, i.e., $P = Q = 0$. Based on this assumption, the configuration of tailsitter VTOL aircraft is shown in Fig. 2. Therefore, based on Equations (6) and (9):

$$\ddot{\phi} = \mathrm{T_l}/\mathrm{J_x} \tag{16}$$

where the exerted torque T_l can be calculated as follows:

$$\mathrm{T_l} = \mathrm{F.d} - \mathrm{C_l}\dot{\phi} \tag{17}$$

The difference between the thrust generated by the right and left rotors is represented by the force ($F = F_1 - F_2$), which is the net force. The distance between the center of mass and each rotor is represented by the parameter "d." Additionally, the aerodynamic damping force $C_l\dot{\phi}$ generates a resisting moment that counteracts the rolling motion, and the damping coefficient C_l is represented by this term.

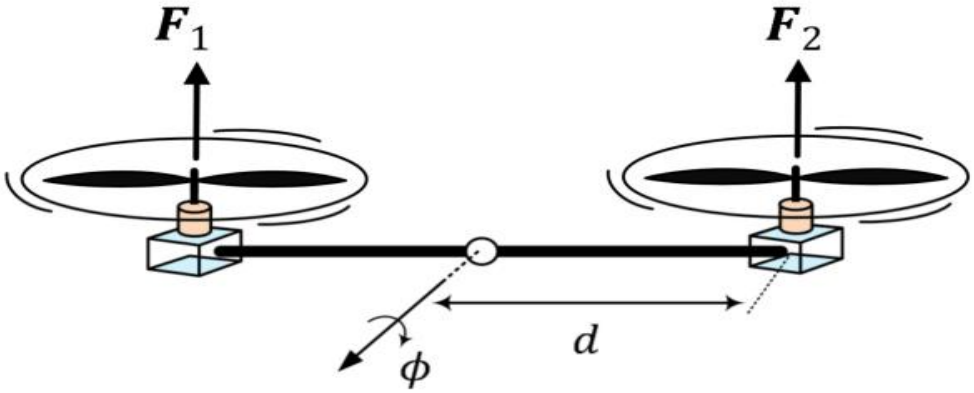

Fig. 2. Configuration of roll dynamics

By combining Equations (14) and (15) and incorporating the effect of gust wind as an uncertainty term $\zeta(t)$ acting on the roll dynamics system, the resulting equation is obtained as follows:

$$\ddot{\phi} = -C_l\dot{\phi} + F.d + \zeta(t) \tag{18}$$

In order to establish the state space of Equation (18), one can let $x_1 = \phi, x_2 = \dot{\phi}$ and $u = F$ to have the following state variable:

$$\begin{bmatrix}\dot{x}_1\\ \dot{x}_2\end{bmatrix} = \begin{bmatrix}0 & 1\\ 0 & -C_l/J_x\end{bmatrix}\begin{bmatrix}x_1\\ x_2\end{bmatrix} + \begin{bmatrix}0\\ d/J_x\end{bmatrix}u + \begin{bmatrix}0\\ \zeta(t)\end{bmatrix} \tag{19}$$

Let the D(t) lump all disturbance, nonlinearity, and uncertainty.

$$D(t) = \zeta(t) + \mathrm{d(t)} + \mathrm{nonlinearity} \tag{20}$$

3. Proposed Controller

The feedback mechanism is steadily advancing to manage a broad spectrum of systems [51]-[57]. In this context, controlling the UAV system involves addressing a range of issues, such as tracking control and handling external disturbances. Particularly, this section explores two control methods to generate the control signals for the UAV system, including Active Disturbance Rejection Control (ADRC) strategy and the conventional Proportional-Integral-Derivative (PID).

3.1. Active Disturbance Rejection Control

ADRC is a powerful control method that can control system contains imprecise information and imprecise internal and external disturbances [58]-[60]. It is also useful for controlling nonlinear systems. The ADRC consists of three basic components: the tracking differentiator (TD), the nonlinear state error feedback (NLSEF), and the ESO. The TD tracks the desired set-point signal, which is used to arrange the transition process, and thus reduces oversight in system regulation. ESO, the core component of the ADRC controller, is primarily used to observe the state feedback of the system and to compensate for interference caused by the extended state. The NLSEF generates control outputs to compensate for all faults in the system. This structure is shown in Fig. 3.

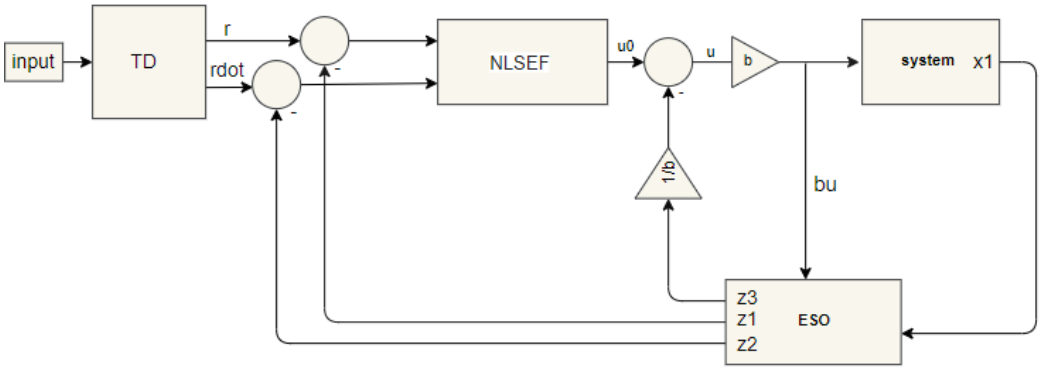

Fig. 3. ADRC structure

According to the concept of ADRC from Fig. 3, the control action is equal to:

$$u = u_0 - z_3/b \tag{21}$$

Where z_3 is the output of ESO and is the summation of uncertainties and nonlinearities affecting the system that will be canceled out in the feedback**,** u_0 can be the output of any suggested controller, for example, PD controller.

$$u_0 = k_p * (r - z_1) - k_d * z_2 \tag{22}$$

This is a simple summary of the concept of ADRC. In the second part, each part of the ADRC will be discussed separately.

3.1.1. Tracking Differentiator (TD)

Most of the time, the TD is used to prevent overshoot and improve system response [61]. It distinguishes and processes the transient profile of the input signals in order to avoid abrupt shifts and instead achieve a gradual increase in output power. As shown in Equation, the TD developed by Zhigao Liu [62] is utilized in this article. Trajectory tracking performance is enhanced by this formulation's superior performance to the traditional differentiator nonlinear tracking formulation, which is simple to implement.

$$\begin{aligned} \dot{x}_1 &= x_2 \\ \dot{x}_2 &= -R^2 \left(a_1[x_1 - v] - b_1 \frac{x_2}{R} - b_2 \frac{{x_2}^n}{R^n} \right) \end{aligned} \tag{23}$$

where $a_1 > 0, b_1 > 0, b_2 > 0, n > 0, n$ is odd.

The desired trajectory and its derivative are represented by $\boldsymbol{x_1}$ and $\boldsymbol{x_2}$. In order to alter the tempo of the transient profile, R is chosen in accordance with the application. The term "tracking differentiator" for v is then applied to the state $\boldsymbol{x_2}$.

3.1.2. Extended State Observer (ESO)

As already mentioned, ESO is an observer who can calculate the states and uncertainties of the system and thus enables disturbances to be compensated or rejected. ESO regards any element that has effects on the plant, including nonlinear dynamics, uncertainties, and external perturbations and coupling effects, as a complete disturbance (extended state) that must be observed and, in this regard, it can be regarded as a disturbance observer or an unknown input observer. The observer is called the Extended State Observer because he regards uncertainty as an extended state. One of its advantages is that it offers comparatively better performance and is easier to execute regardless of the plant's mathematical model. This study presents the LESO, NLESO, and FESO strategies.

A. Linear Extended State Observer (LESO)

It is the simplest type of ESO, multiplying the error by the gain. Expresses the LESO equations

$$\begin{aligned} \dot{\hat{z}}_1 &= \hat{z}_2 + \beta_1(e) \\ \dot{\hat{z}}_2 &= \hat{z}_3 + \beta_2(e) \\ &\vdots \\ \dot{\hat{z}}_n &= \hat{z}_{n+1} + \beta_n(e) + b_o u \\ \dot{\hat{z}}_{n+1} &= \beta_{n+1}(e) \end{aligned} \tag{24}$$

where ϵ is a small valve the observer states (z_1, ..., z_n) function to estimate the actual states of the system (x_1, ..., x_n), whereas the state of observer z_{n+1} is tasked with estimating the aggregated uncertainty h(x). The parameters [$\beta_1, \ldots., \beta_{n+1}$] are positive constants.

$$e = y - \hat{z}_1 \tag{25}$$

To verify that the polynomial($s^{n+1} + \beta_1 s^n \ldots.. + \beta_{n+1}$)is Hurwitz. The following goal from the designed observer $z_1 \longrightarrow x_1, \ldots., z_{n+1} \longrightarrow h(x)$ as $t \longrightarrow \infty$.

B. Nonlinear Extended State Observer (NESO)

In the second version of ESO, this type is considered more complex than the first version because it contains more variables. This type can be expressed using the following equations:

$$\begin{aligned} \dot{\hat{z}}_1 &= \hat{z}_2 + \beta_1 g_1(e) \\ \dot{\hat{z}}_2 &= \hat{z}_3 + \beta_2 g_2(e) \\ &\vdots \\ \dot{\hat{z}}_n &= \hat{z}_{n+1} + \beta_n g_n(e) + b_o u \\ \dot{\hat{z}}_{n+1} &= \beta_{n+1} g_{n+1}(e) \end{aligned} \tag{26}$$

$g_i(.)$are a set of appropriately constructed nonlinear gain functions satisfying $e \cdot g_i(e) > 0$, for all $e \neq 0$and $g_i(0) = 0$. With a suitable choice of nonlinear functions $g_i(.)$ and their associated parameters, it is expected that the estimated state variables z_i will converge to the actual system states z_i, i.e., $z_i \rightarrow z_i$; for $i = 1,2, \ldots, n+1$. An essential part of ESO design is selecting the nonlinear function. Based on the results of experiments, the general formulation of these functions was chosen empirically [63]-[64].

$$g_i(e, \alpha_i, \delta) = \begin{cases} |e|^{\alpha_i} \text{sign}(e), & |e| > \delta \\ \dfrac{e}{\delta^{1-\alpha_i}}, & |e| \leq \delta \end{cases} \quad i = 1,2, \ldots, n+1 \tag{27}$$

where δ is greater than zero. It is evident that $g_i(.)$ is a nonlinear function that exhibits a linear behavior in the vicinity of the origin. This function leverages nonlinear feedback properties for large signals while mitigating chattering, which is commonly observed in sliding mode observers, by avoiding proximity to the origin. A key characteristic of these functions is that, for $0<\alpha_i<1$, $g_i(.)$ generates a low gain when the error is large and a relatively higher gain when the error is small. The benefit is limited by the constant δ_i, which is a tiny value. In the vicinity of the origin and establishes the error range that corresponds to high gain. The observer gain is parameterized as $\beta_1 = 3\mathrm{w_n}; \beta_2 = 3\mathrm{w_n^2}; \beta_3 = \mathrm{w_n^3}$.

C. Fractional Extended State Observer (FESO)

The latest version of ESO, show in Fig. 4, Fractional-Order Extended State Observers (FOESO), has shown promising results in various control applications. They offer improved performance and higher estimation accuracy compared to full-order observers [65]-[66].

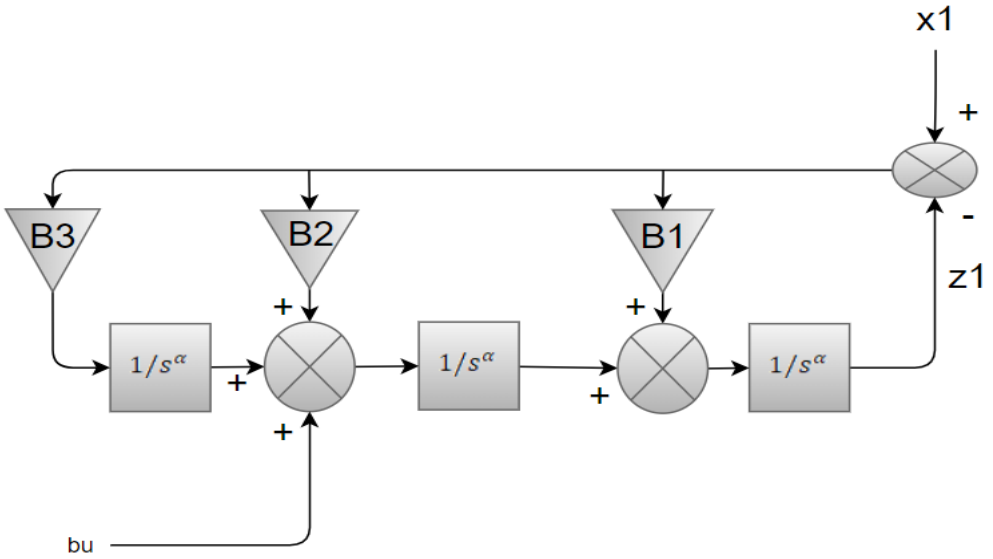

Fig. 4. Block diagram of Fractional-order ESO structure

An extension of the integration and differentiation methods to an operator that is not an integer is the fraction calculation (27):

$$D^{\alpha} = \begin{cases} \dfrac{d^{\alpha}}{d_t^{\alpha}} & \text{for } \alpha \succ 0 \\ 1 & \text{for } \alpha = 0 \\ \displaystyle\int_a^t (dt)^{-\alpha} & \text{for } \alpha \prec 0 \end{cases} \tag{28}$$

where (α) represents the fractional order, which ranges from 0 to 1, and a and t represent the operation's limitations. The fractional-order derivative can be applied to all estimated states of the observer. Therefore, it is possible to utilize the fractional-order derivative for all estimated states of the observer, represented as $\hat{z} = [\hat{z}_1, \hat{z}_2, \ldots \ldots, \hat{z}_n, \hat{z}_{n+1}]$. Expresses equations of this type.

$$\begin{gathered} D^{\alpha_f}\hat{z}_n = \hat{z}_{n+1} + bu + \beta_n(x_1 - \hat{z}_1) \\ D^{\alpha_f}\hat{z}_{n+1} = \beta_{n+1}(x_1 - \hat{z}_1) \\ \hat{y}_1 = c\hat{z}_1 \end{gathered} \tag{29}$$

The parameters α and observers gains $[\beta_1, \ldots. \beta_{n+1},]$ are positive constants chosen by using trial and error. The extended observer's characteristic polynomial satisfies:

$$\mathrm{s}^{3\alpha} + \beta_1\, \mathrm{s}^{2\alpha} + \beta_2\, \mathrm{s}^{\alpha} + \beta_3 = (\mathrm{s}^{\alpha} + \mathrm{w_o})^3 \tag{30}$$

Thus, the observer gain is parameterized as $\beta_1 = 3w_o$; $\beta_2 = 3w_o^2$; $\beta_3 = w_o^3$. The fractional order extended state observer's parameter adjustment procedure is made simple by the fact that the to be adjusted parameters are clearly linked to the bandwidth w_o.

D. Nonlinear state error feedback (NLSEF)

Fig. 3 illustrates the design of the ADRC. Based on Fig. 3, ADRC contains a set of three units: Tracking Differentiator, ESO, and Nonlinear state error feedback. The control law is defined as.

$$u(t) = u_0(t) - z_3(t)/b_0 \tag{31}$$

This simplifies the plant into a double integrator, which is then managed by the nonlinear PD controller.

$$u_0(t) = k_P f_1(e_1) + k_D f_2(\dot{e}_1) \tag{32}$$

k_P and k_D are the gains of the PD controller, andf_1 (.) and f_2 () are appropriate nonlinear functions, such as the one in (27). where e_1=$v_1 - x_1$ and $\dot{e}_1$is the derivative of error, are position error and velocity error, respectively. The values of the variables can be obtained by: trial and error or use optimization methods in this paper using trial and error.

3.2. PID Controller

Proportional-Integral-Derivative (PID) controller is the most commonplace control method utilized in industry and has been universally regular in industrial applications. The popularity of PID controllers can be attributed partly to their strong performance in an extensive variety of working situations and in part to their functional simplicity, which permits engineers to operate them in an easy, truthful way. The general structure of the PID controller is shown in Fig. 5.

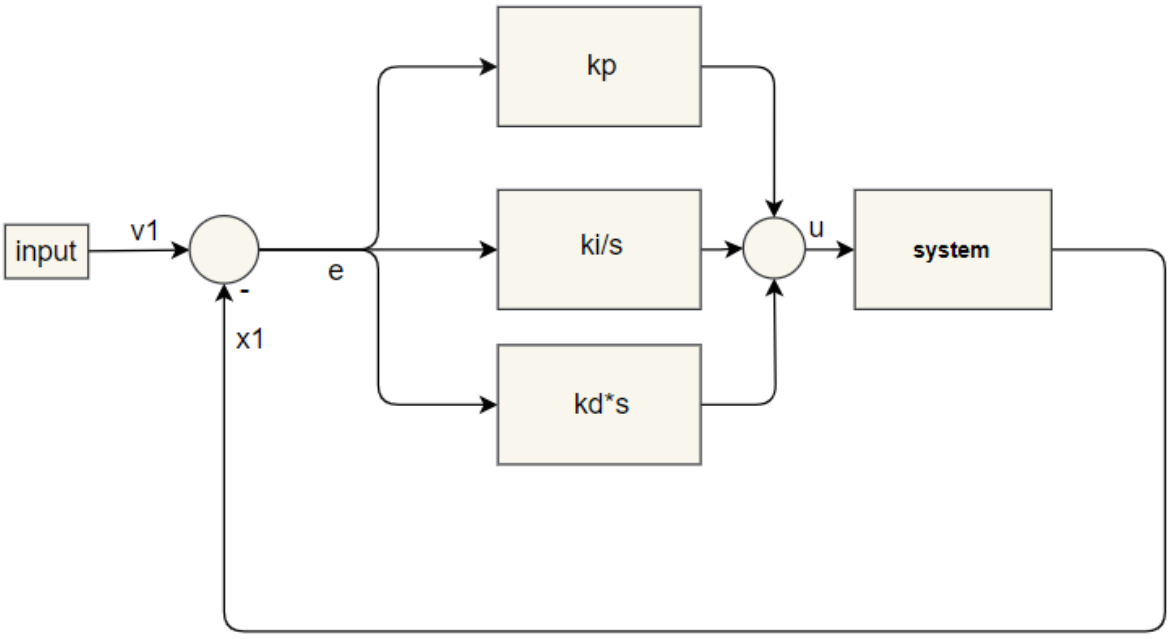

Fig. 5. Block diagram of PID controller

The control law is defined as [67]-[68]:

$$u(t) = K_p e(t) + K_i \int_0^t e(\tau)d\tau + K_d \frac{de(t)}{dt} \tag{33}$$

where K_p, K_i, and K_d, denote the gains for the proportional, integral, and derivative terms respectively. Gain values can be obtained using any adjustment methods such, Ziegler-Nichols, Trial and error, and Cohen-Coon.

4. Simulation Results

The effectiveness of the proposed controller and extended condition observer to control the roll motion of the UAV was verified using simulation results using MATLAB (R2020a). The parameters of the system are listed in Table 1. This section is divided into two parts. The first part focuses on using three ESO types with the aim of finding out which has the lowest estimation error. The comparison criterion will be the root mean square error (RMSE). In the second part, the observer with the best performance is selected and the ADRC method is applied to it. This method is then compared with the traditional PID method. The best approach is determined using the verification method that results in the fewest tracking errors. In addition, a criterion, in particular the RMSE is used for the evaluation. The parameters of each TD, LESO, NESO, FOESO, NPD and PID are given in (Table 2, Table 3, Table 4, Table 5, Table 6, and Table 7). These values were obtained using the trial-and-error method.

Table 1. Parameters value of system

Parameter	Value
J_x	0.0144 kg.m^2
C_l	0.36
d	0.2 m

Table 2. Parameter value of tracking differentiator

Parameter	Value
$v(t)$	$10step(t-1)$
R	8
b_1	3
b_2	0.01
n	1
a	2

Table 3. Parameter value of LESO

Parameter	Value
w_l	977.93
β_1	$3w_l$
β_2	$3w_l^2$
β_3	w_l^3

Table 4. Parameter value of NESO

Parameter	Value
w_o	986
β_1	$3w_o$
β_2	$3w_o^2$
β_3	w_o^3
$[\alpha_1, \alpha_2, \alpha_3]$	[0.9930,0.9980,0.999]

4.1. Estimation Error

In this part, the examination of the three types of ESO and choose the best one is given. The selection of the best ESO is determined based on the RMES which is given in equation (34) [69]-[70].

$$RMSE = \sqrt{\sum_{i=1}^{n} \frac{(\hat{x}_i - x_i)^2}{n}} \tag{34}$$

In this step, the system is operates without controller (open loop), the input (v_0) and reference signal (v_1) from Tracking Differentiator (TD) show Fig. 6. The system with LESO is shown Fig. 7

(a, b, c), The system with NESO is shown in Fig. 8 (a, b, c), The system with FOESO is shown in Fig. 9 (a, b, c).

Table 5. Parameter value of FOESO

Parameter	Value
w_n	892
β_1	$3w_n$
β_2	$3w_n^2$
β_3	w_n^3
δ	0.01
$[\alpha_1, \alpha_2, \alpha_3]$	[0.7,0.8,0.9]

Table 6. Parameter value of NPD Controller

Parameter	Value
k_P	270
k_d	100
α_1, α_2	1
δ	0000001

Table 7. Parameter value of PID Controller

Parameter	Value
k_P	600
k_i	1
k_d	4

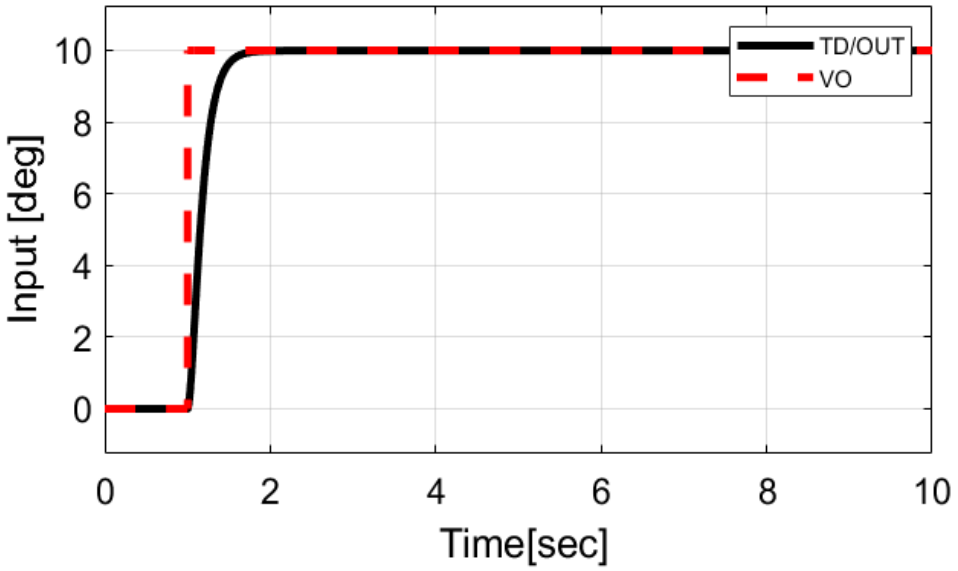

Fig. 6. Output from TD (v_1)

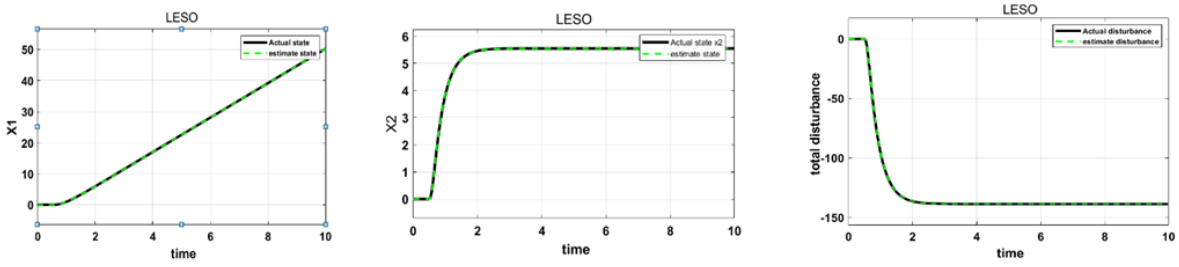

a b c

Fig. 7. LESO

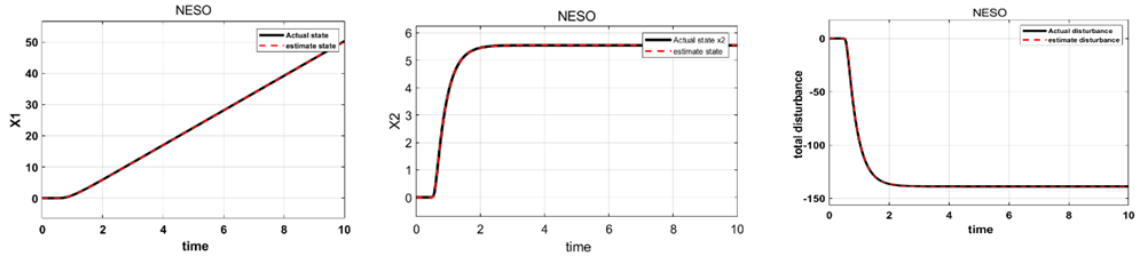

a b c

Fig. 8. NESO

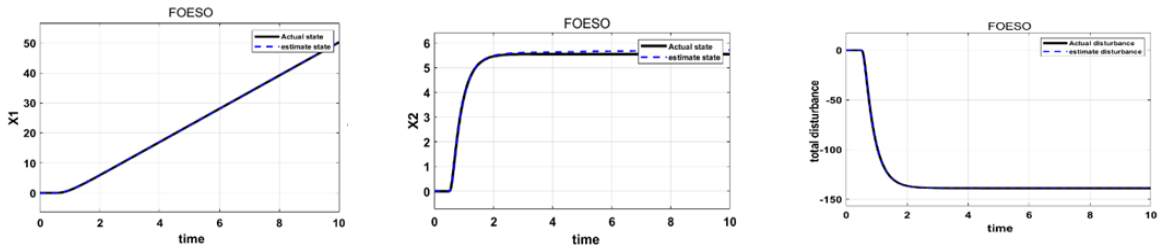

a b c

Fig. 9. FOESO

It can be seen from (Fig. 6, Fig. 7 and Fig. 8) that all types of observers work properly. However, the best ones using the RMSE benchmark function as shown in the Table 8.

Table 8. RMSE of estimation error of observers (LESO, NESO and FOESO)

Estimation error	LESO	NESO	FOESO
$x_1 - \hat{x}_1$	7.2736e-10	6.3450e-08	1.5890e-08
$x_2 - \hat{x}_2$	1.6652e-05	1.7032e-04	0.0903
$D(t) - \hat{x}_3$	0.0305	0.1529	0.0706

From the above table, the best estimator for this system is LESO, which will be applied with NPD to form ADRC.

4.2. Tracking Error

In this part, ADRC and PID controllers are augmented to the system for two cases: with disturbance and without disturbance. Then, the performance of the two controllers were evaluated using RMSE criterion for the desired reference (v_1) as in Fig. 6.

4.2.1. Without Disturbance

It can be seen from Fig. 10 that both controllers were capable to follow the desired input. However, the ADRC controller's control signal, as depicted in Fig. 11, is better that the control signal of the PID controller. The control signal of the PID controller was higher and greater oscillatory. This suggests that ADRC plays better in this situation. Furthermore, based on the RMSE values, ADRC has lower RMSE as proven in Table 9.

Table 9. RMSE of estimation error of controller (PID and ADRC)

Controller	RMSE (tracking error)
PID	0.01707
ADRC	0.003226

4.2.2. With Disturbance

The disturbance signal, as defined in Eq. (35) and illustrated in Fig. 12. is applied to both the PID controller and ADRC.

$$D(t) = (\sin(2\pi \times 0.02t) + \sin(2\pi \times 0.05t) + \sin(2\pi \times 0.09t)) \quad (35)$$

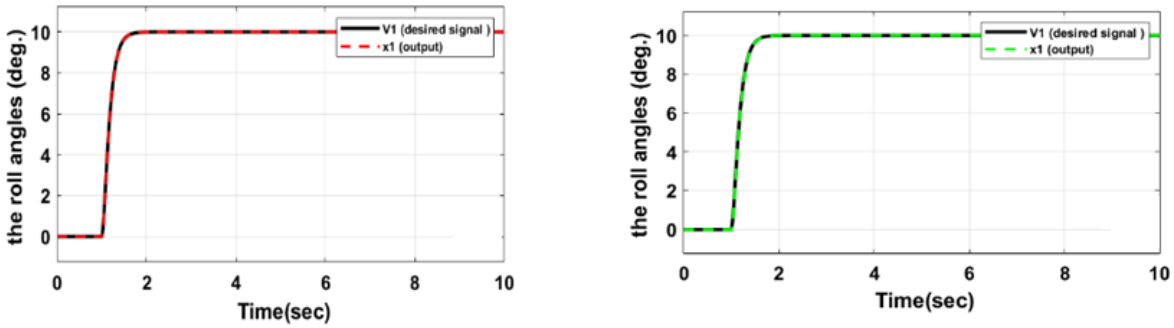

Fig. 10. Roll angle (dag) in (a using ADRC) and (b using PID)

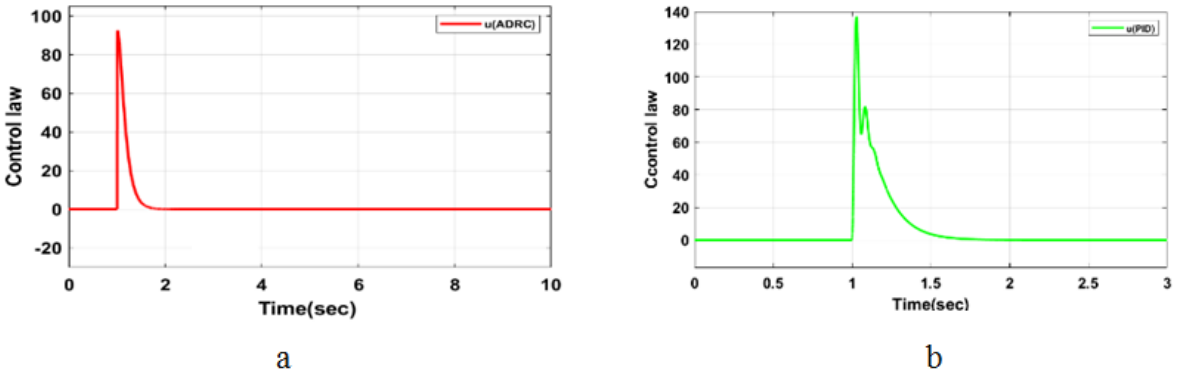

Fig. 11. Control law in (a) ADRC and (b) PID

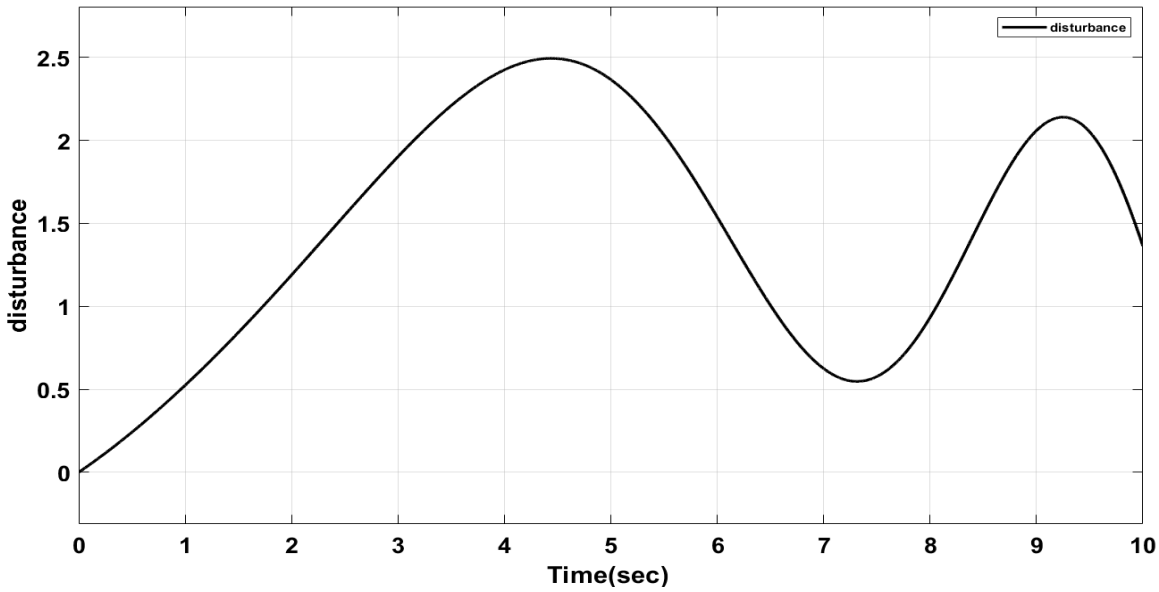

Fig. 12. Disturbance signal

It can be seen from Fig. 13 that the ADRC response is superior, with a decrease overshoot in comparison to the PID controller. Moreover, Fig. 14 a demonstrates that the control motion for ADRC is significantly lower than that for PID, as further highlighted in Fig. 14 b. Additionally, the RMSE value for the ADRC is less than the PID controller as presented in the Table 10. The aforementioned simulation results demonstrate that the ADRC with LESO is capable of effectively controlling the UAV in a better manner than that of the PID controller.

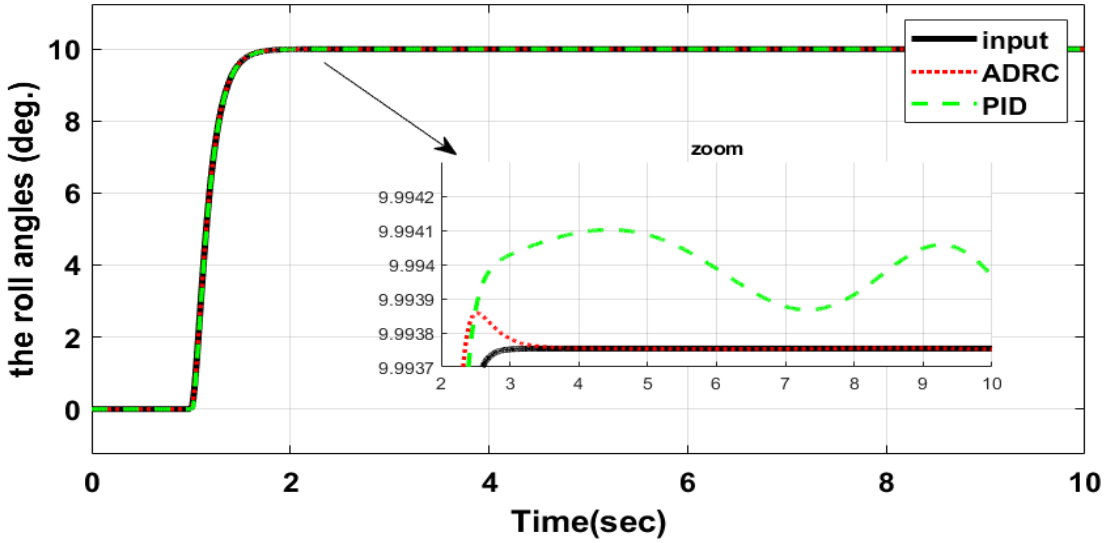

Fig. 13. Roll angle (dag) for ADRC and PID with disturbance

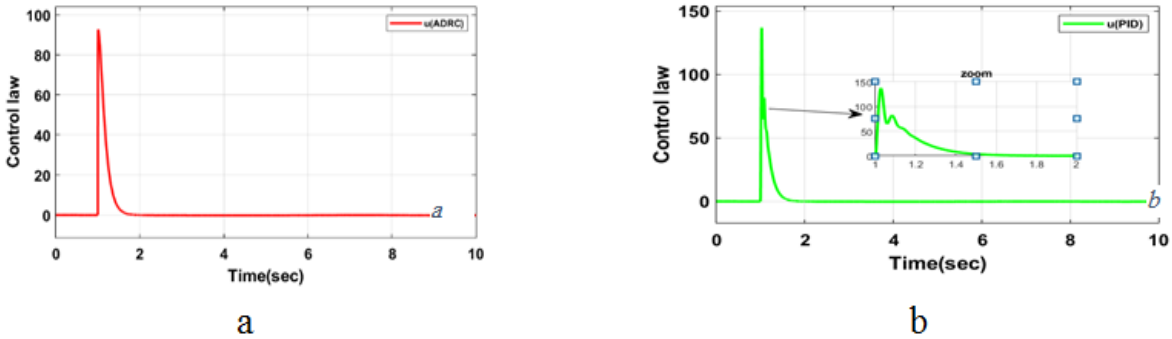

a b

Fig. 14. Control law in (a) ADRC and (b) PID with disturbance

Table 10. RMSE of estimation error of controller (PID and ADRC)

Controller	RMSE (tracking error)
PID	0.01709
ADRC	0.003228

5. Conclusion

This paper presented a comparative study of different observer types within an Active Disturbance Rejection Control (ADRC) framework for improving roll motion control of a VTOL-UAV. The first part of the results focused on estimating the system states and lumped disturbances using LESO, NESO, and FOESO, with LESO demonstrating the lowest estimation error based on the RMSE criterion. Building upon this, the second part of the study is evaluated two control strategies—ADRC (incorporating LESO and an NPD controller) and a conventional PID controller—under both disturbance-free and disturbed conditions. The simulation outcomes revealed that ADRC not only provided faster response and lower overshoot but also achieved lower RMSE values in tracking the desired roll angle. These findings underscore the robustness of ADRC in handling uncertainties and external disturbances, making it a compelling choice for advanced UAV applications. Future work may explore integrating optimization-based tuning methods or extending the proposed framework to multi-rotor systems and other flight maneuvers, thereby further enhancing the adaptability and resilience of UAV control strategies.

Author Contribution: All authors contributed equally to the main contributor to this paper. All authors read and approved the final paper.

Funding: This research received no external funding.

Conflicts of Interest: The authors declare no conflict of interest.

References

[1] S. Hayat, E. Yanmaz and R. Muzaffar, "Survey on Unmanned Aerial Vehicle Networks for Civil Applications: A Communications Viewpoint," *IEEE Communications Surveys & Tutorials*, vol. 18, no. 4, pp. 2624-2661, 2016, https://doi.org/10.1109/COMST.2016.2560343.

[2] H. Shakhatreh *et al*., "Unmanned Aerial Vehicles (UAVs): A Survey on Civil Applications and Key Research Challenges," *IEEE Access*, vol. 7, pp. 48572-48634, 2019, https://doi.org/10.1109/ACCESS.2019.2909530.

[3] M. Mozaffari, W. Saad, M. Bennis, Y. -H. Nam and M. Debbah, "A Tutorial on UAVs for Wireless Networks: Applications, Challenges, and Open Problems," *IEEE Communications Surveys & Tutorials*, vol. 21, no. 3, pp. 2334-2360, 2019, https://doi.org/10.1109/COMST.2019.2902862.

[4] L. Gupta, R. Jain and G. Vaszkun, "Survey of Important Issues in UAV Communication Networks," *IEEE Communications Surveys & Tutorials*, vol. 18, no. 2, pp. 1123-1152, 2016, https://doi.org/10.1109/COMST.2015.2495297.

[5] A. Fotouhi *et al*., "Survey on UAV Cellular Communications: Practical Aspects, Standardization Advancements, Regulation, and Security Challenges," *IEEE Communications Surveys & Tutorials*, vol. 21, no. 4, pp. 3417-3442, 2019, https://doi.org/10.1109/COMST.2019.2906228.

[6] N. Hossein Motlagh, T. Taleb and O. Arouk, "Low-Altitude Unmanned Aerial Vehicles-Based Internet of Things Services: Comprehensive Survey and Future Perspectives," *IEEE Internet of Things Journal*, vol. 3, no. 6, pp. 899-922, 2016, https://doi.org/10.1109/JIOT.2016.2612119.

[7] Y. Zeng, R. Zhang and T. J. Lim, "Wireless communications with unmanned aerial vehicles: opportunities and challenges," *IEEE Communications Magazine*, vol. 54, no. 5, pp. 36-42, 2016, https://doi.org/10.1109/MCOM.2016.7470933.

[8] V. Roberge, M. Tarbouchi and G. Labonté, "Fast Genetic Algorithm Path Planner for Fixed-Wing Military UAV Using GPU," *IEEE Transactions on Aerospace and Electronic Systems*, vol. 54, no. 5, pp. 2105-2117, 2018, https://doi.org/10.1109/TAES.2018.2807558.

[9] E. T. Alotaibi, S. S. Alqefari and A. Koubaa, "LSAR: Multi-UAV Collaboration for Search and Rescue Missions," *IEEE Access*, vol. 7, pp. 55817-55832, 2019, https://doi.org/10.1109/ACCESS.2019.2912306.

[10] M. A. Rahman, S. Azad, A. T. Asyhari, M. Z. A. Bhuiyan and K. Anwar, "Collab-SAR: A Collaborative Avalanche Search-and-Rescue Missions Exploiting Hostile Alpine Networks," *IEEE Access*, vol. 6, pp. 42094-42107, 2018, https://doi.org/10.1109/ACCESS.2018.2848366.

[11] N. Geng, Q. Meng, D. Gong and P. W. H. Chung, "How Good are Distributed Allocation Algorithms for Solving Urban Search and Rescue Problems? A Comparative Study With Centralized Algorithms," *IEEE Transactions on Automation Science and Engineering*, vol. 16, no. 1, pp. 478-485, 2019, https://doi.org/10.1109/TASE.2018.2866395.

[12] S. V. Sibanyoni, D. T. Ramotsoela, B. J. Silva, and G. P. Hancke, "A 2-d acoustic source localization system for drones in search and rescue missions," *IEEE Sensors Journal*, vol. 19, pp. 332–341, 2019, https://doi.org/10.1109/JSEN.2018.2875864.

[13] D. Murugan, A. Garg and D. Singh, "Development of an Adaptive Approach for Precision Agriculture Monitoring with Drone and Satellite Data," *IEEE Journal of Selected Topics in Applied Earth Observations and Remote Sensing*, vol. 10, no. 12, pp. 5322-5328, 2017, https://doi.org/10.1109/JSTARS.2017.2746185.

[14] X. He *et al*., "Autonomous Chemical-Sensing Aerial Robot for Urban/Suburban Environmental Monitoring," *IEEE Systems Journal*, vol. 13, no. 3, pp. 3524-3535, 2019, https://doi.org/10.1109/JSYST.2019.2905807.

[15] Z. Lin, H. H. T. Liu and M. Wotton, "Kalman Filter-Based Large-Scale Wildfire Monitoring With a System of UAVs," *IEEE Transactions on Industrial Electronics*, vol. 66, no. 1, pp. 606-615, 2019, https://doi.org/10.1109/TIE.2018.2823658.

[16] K. Kuru, D. Ansell, W. Khan and H. Yetgin, "Analysis and Optimization of Unmanned Aerial Vehicle Swarms in Logistics: An Intelligent Delivery Platform," *IEEE Access*, vol. 7, pp. 15804-15831, 2019, https://doi.org/10.1109/ACCESS.2019.2892716.

[17] S. Sawadsitang, D. Niyato, P. -S. Tan and P. Wang, "Joint Ground and Aerial Package Delivery Services: A Stochastic Optimization Approach," *IEEE Transactions on Intelligent Transportation Systems*, vol. 20, no. 6, pp. 2241-2254, 2019, https://doi.org/10.1109/TITS.2018.2865893.

[18] K. Peng *et al*., "A Hybrid Genetic Algorithm on Routing and Scheduling for Vehicle-Assisted Multi-Drone Parcel Delivery," *IEEE Access*, vol. 7, pp. 49191-49200, 2019, https://doi.org/10.1109/ACCESS.2019.2910134.

[19] K. Dorling, J. Heinrichs, G. G. Messier and S. Magierowski, "Vehicle Routing Problems for Drone Delivery," *IEEE Transactions on Systems, Man, and Cybernetics: Systems*, vol. 47, no. 1, pp. 70-85, 2017, https://doi.org/10.1109/TSMC.2016.2582745.

[20] Y. Li, B. Peng, L. He, K. Fan and L. Tong, "Road Segmentation of Unmanned Aerial Vehicle Remote Sensing Images Using Adversarial Network With Multiscale Context Aggregation," *IEEE Journal of Selected Topics in Applied Earth Observations and Remote Sensing*, vol. 12, no. 7, pp. 2279-2287, 2019, https://doi.org/10.1109/JSTARS.2019.2909478.

[21] L. Deng, X. Hao, Z. Mao, Y. Yan, J. Sun and A. Zhang, "A Subband Radiometric Calibration Method for UAV-Based Multispectral Remote Sensing," *IEEE Journal of Selected Topics in Applied Earth Observations and Remote Sensing*, vol. 11, no. 8, pp. 2869-2880, 2018, https://doi.org/10.1109/JSTARS.2018.2842466.

[22] A. H. Sawalmeh, N. S. Othman, H. Shakhatreh and A. Khreishah, "Wireless Coverage for Mobile Users in Dynamic Environments Using UAV," *IEEE Access*, vol. 7, pp. 126376-126390, 2019, https://doi.org/10.1109/ACCESS.2019.2938272.

[23] J. Cui, H. Shakhatreh, B. Hu, S. Chen and C. Wang, "Power-Efficient Deployment of a UAV for Emergency Indoor Wireless Coverage," *IEEE Access*, vol. 6, pp. 73200-73209, 2018, https://doi.org/10.1109/ACCESS.2018.2882896.

[24] X. Zhang and L. Duan, "Fast Deployment of UAV Networks for Optimal Wireless Coverage," *IEEE Transactions on Mobile Computing*, vol. 18, no. 3, pp. 588-601, 2019, https://doi.org/10.1109/TMC.2018.2840143.

[25] H. Kim and J. Ben-Othman, "A Collision-Free Surveillance System Using Smart UAVs in Multi Domain IoT," *IEEE Communications Letters*, vol. 22, no. 12, pp. 2587-2590, 2018, https://doi.org/10.1109/LCOMM.2018.2875477.

[26] T. Yu, X. Wang and A. Shami, "UAV-Enabled Spatial Data Sampling in Large-Scale IoT Systems Using Denoising Autoencoder Neural Network," *IEEE Internet of Things Journal*, vol. 6, no. 2, pp. 1856-1865, 2019, https://doi.org/10.1109/JIOT.2018.2876695.

[27] N. H. Motlagh, M. Bagaa and T. Taleb, "Energy and Delay Aware Task Assignment Mechanism for UAV-Based IoT Platform," *IEEE Internet of Things Journal*, vol. 6, no. 4, pp. 6523-6536, 2019, https://doi.org/10.1109/JIOT.2019.2907873.

[28] J. Chakareski, "UAV-IoT for Next Generation Virtual Reality," *IEEE Transactions on Image Processing*, vol. 28, no. 12, pp. 5977-5990, 2019, https://doi.org/10.1109/TIP.2019.2921869.

[29] V. Sharma, R. Kumar, and R. Kaur, "UAV-Assisted Content-Based Sensor Search in IoTs," *Electronics Letters*, vol. 53, no. 11, pp. 696-754, 2017, https://doi.org/10.1049/el.2016.3487.

[30] M. A. Abd-Elmagid and H. S. Dhillon, "Average Peak Age-of-Information Minimization in UAV-Assisted IoT Networks," *IEEE Transactions on Vehicular Technology*, vol. 68, no. 2, pp. 2003-2008, 2019, https://doi.org/10.1109/TVT.2018.2885871.

[31] Z. Gao, "Active disturbance rejection control: a paradigm shift in feedback control system design," *2006 American Control Conference*, p. 7, 2006, https://doi.org/10.1109/ACC.2006.1656579.

[32] N. A. Alawad, A. J. Humaidi, A S. Alaraji, "Sliding Mode-Based Active Disturbance Rejection Control of Assistive Exoskeleton Device for Rehabilitation of Disabled Lower Limbs," *Anais da Academia Brasileira de Ciências*, vol. 95, no. 2, p. e20220680, 2023, https://doi.org/10.1590/0001-3765202320220680.

[33] N. A. Alawad, A. J. Humaidi, A. S. M. Al-Obaidi, A. S. Alaraji, "Active Disturbance Rejection Control of Wearable Lower-Limb System Based on Reduced ESO," *Indonesian Journal of Science and Technology*, vol. 7, no. 2, pp. 203-218, 2022, https://doi.org/10.17509/ijost.v7i2.46435.

[34] N. A. Alawad, A. J. Humaidi, A. S. Al-Araji, "Improved Active Disturbance Rejection Control for the Knee Joint Motion Model," *Mathematical Modelling of Engineering Problems*, vol. 9, no. 2, pp. 477-483, 2022, https://doi.org/10.18280/mmep.090225.

[35] N. A. Alawad, A. J. Humaidi, A. S. Alaraji, "Design of Active Disturbance Rejection Control for Rehabilitation-Assistant Device of Lower Limbs under Cross Coupling Effect," *Proceedings of the Institution of Mechanical Engineers, Part C: Journal of Mechanical Engineering Science*, vol. 238, no. 15, pp. 7388-7398, 2024, https://doi.org/10.1177/09544062241232230.

[36] A. J. Humaidi, H. M. Badr and A. H. Hameed, "PSO-Based Active Disturbance Rejection Control for Position Control of Magnetic Levitation System," *2018 5th International Conference on Control, Decision and Information Technologies (CoDIT)*, pp. 922-928, 2018, https://doi.org/10.1109/CoDIT.2018.8394955.

[37] R. Parvathy and A. E. Daniel, "A survey on active disturbance rejection control," *2013 International Mutli-Conference on Automation, Computing, Communication, Control and Compressed Sensing (iMac4s)*, pp. 330-335, 2013, https://doi.org/10.1109/iMac4s.2013.6526432.

[38] G. Tian and Z. Gao, "Frequency Response Analysis of Active Disturbance Rejection Based Control System," *2007 IEEE International Conference on Control Applications*, pp. 1595-1599, 2007, https://doi.org/10.1109/CCA.2007.4389465.

[39] M. Ramírez-Neria, J. Morales-Valdez, W. Yu, "Active vibration control of building structure using active disturbance rejection control," *Journal of Vibration and Control*, vol. 28, no. 17-18, pp. 2171-2186, 2021, https://doi.org/10.1177/10775463211009377.

[40] D. Sun, "Comments on Active Disturbance Rejection Control," *IEEE Transactions on Industrial Electronics*, vol. 54, no. 6, pp. 3428-3429, 2007, https://doi.org/10.1109/TIE.2007.909047.

[41] H. Qi, S.-J. Cao, J.-Y. Wu, Y.-M. Peng, H. Nie, X.-H. Wei, "Research on the Effect Characteristics of Free-Tail Layout Parameters on Tail-Sitter VTOL UAVs," *Agriculture*, vol. 14, no. 3, p. 472, 2024, https://doi.org/10.3390/agriculture14030472.

[42] B. Li, W. Zhou, J. Sun, C.-Y. Wen, and C.-K. Chen, "Development of model predictive controller for a Tail-Sitter VTOL UAV in hover flight," *Sensors*, vol. 18, no. 9, pp. 2859-2879, 2018, https://doi.org/10.3390/s18092859.

[43] J. A. Guerrero, R. Lozano, G. Romero, D. Lara-Alabazares and K. C. Wong, "Robust control design based on sliding mode control for hover flight of a mini tail-sitter Unmanned Aerial Vehicle," *2009 35th Annual Conference of IEEE Industrial Electronics*, pp. 2342-2347, 2009, https://doi.org/10.1109/IECON.2009.5415267.

[44] X. Lyu, J. Zhou, H. Gu, Z. Li, S. Shen and F. Zhang, "Disturbance Observer Based Hovering Control of Quadrotor Tail-Sitter VTOL UAVs Using H∞ Synthesis," *IEEE Robotics and Automation Letters*, vol. 3, no. 4, pp. 2910-2917, 2018, https://doi.org/10.1109/LRA.2018.2847405.

[45] Y. Yang, J. Zhu, X. Zhang and X. Wang, "Active Disturbance Rejection Control of a Flying-Wing Tailsitter in Hover Flight," *2018 IEEE/RSJ International Conference on Intelligent Robots and Systems (IROS)*, pp. 6390-6396, 2018, https://doi.org/10.1109/IROS.2018.8594470.

[46] Z. Li, L. Zhang, H. Liu, Z. Zuo, and C. Liu, "Nonlinear robust control of tail-sitter aircrafts in flight mode transitions," *Aerospace Science and Technology*, vol. 81, pp. 348-361, 2018, https://doi.org/10.1016/j.ast.2018.08.021.

[47] G. Haisheng and L. Jinkun, "Sliding Mode Control for VTOL Aircraft Based on High-Gain Observer," *2012 Second International Conference on Instrumentation, Measurement, Computer, Communication and Control*, pp. 305-309, 2012, https://doi.org/10.1109/IMCCC.2012.75.

[48] A. Flores, A. M. de Oca and G. Flores, "A Simple Controller for the Transition Maneuver of a Tail-Sitter Drone," *2018 IEEE Conference on Decision and Control (CDC)*, pp. 4277-4281, 2018, https://doi.org/10.1109/CDC.2018.8619303.

[49] F. Çakici, M. Kemal, "Control System Design of a Vertical Take-off and Landing Fixed-Wing UAV," *IFAC-PapersOnLine*, vol. 49, pp. 267–272, 2016, https://doi.org/10.1016/j.ifacol.2016.07.045.

[50] K. C. Wong, J. A. Guerrero, D. Lara and R. Lozano, "Attitude stabilization in hover flight of a mini tail-sitter UAV with variable pitch propeller," *2007 IEEE/RSJ International Conference on Intelligent Robots and Systems*, pp. 2642-2647, 2007, https://doi.org/10.1109/IROS.2007.4399278.

[51] B. L. Stevens, F. L. Lewis, E. N. Johnson, "Aircraft Control and Simulation: Dynamics, Controls Design, and Autonomous Systems," *John Wiley & Sons*, 2016, https://doi.org/10.1002/9781119174882.

[52] A. K. Ahmed, H. Al-Khazraji, and S. M. Raafat, "Optimized PI-PD control for varying time delay systems based on modified Smith predictor," *International Journal of Intelligent Engineering and Systems*, vol. 17, no. 1, pp. 331-342, 2024, https://doi.org/10.22266/ijies2024.0229.30.

[53] H. Al-Khazraji, K. Al-Badri, R. Al-Majeez, and A.J. Humaidi, "Synergetic Control-Based Sea Lion Optimization Approach for Position Tracking Control of Ball and Beam System," *International Journal of Robotics and Control Systems*, vol. 4, no. 4, pp. 1547-1560, 2024, https://doi.org/10.31763/ijrcs.v4i4.1551.

[54] B. M. Nguyen, T. Tran, T. Nguyen, G. Nguyen, "An improved sea lion optimization for workload elasticity prediction with neural networks," *International Journal of Computational Intelligence Systems*, vol. 15, no. 1, p. 90, 2020, https://doi.org/10.1007/s44196-022-00156-8.

[55] M. Q. Kadhim, F. R. Yaseen, H. Al-Khazraji and A. J. Humaidi, "Application of Terminal Synergetic Control Based Water Strider Optimizer for Magnetic Bearing Systems," *Journal of Robotics and Control (JRC)*, vol. 5, no. 6, pp. 1973-1979, 2024, https://doi.org/10.18196/jrc.v5i6.23867.

[56] F. R. Al-Ani, O. F. Lutfy and H. Al-Khazraji, "Optimal Backstepping and Feedback Linearization Controllers Design for Tracking Control of Magnetic Levitation System: A Comparative Study," *Journal of Robotics and Control (JRC)*, vol. 5, no. 6, pp. 1888-1896, 2024, https://doi.org/10.18196/jrc.v5i6.24073.

[57] H. Al-Khazraji, W. Guo and A. J. Humaidi, "Improved Cuckoo Search Optimization for Production Inventory Control Systems," *Serbian Journal of Electrical Engineering*, vol. 21, no. 2, pp. 187-200, 2024, https://doi.org/10.2298/SJEE2402187A.

[58] H. Al-Khazraji, R. M. Naji and M. K. Khashan, "Optimization of Sliding Mode and Back-Stepping Controllers for AMB Systems Using Gorilla Troops Algorithm," *Journal Européen des Systèmes Automatisés*, vol. 57, no. 2, pp. 417–424, 2024, https://doi.org/10.18280/jesa.570211.

[59] N. A. Alawad, A. J. Humaidi, M. M. Muslim, "Modified ADRC for position lower-knee exoskeleton system: Rehabilitation case," *International Review of Applied Sciences and Engineering*, pp. 1-10, 2025, https://doi.org/10.1556/1848.2024.00922.

[60] A. J. Humaidi, H. M. Badr and A. R. Ajil, "Design of Active Disturbance Rejection Control for Single-Link Flexible Joint Robot Manipulator," *2018 22nd International Conference on System Theory, Control and Computing (ICSTCC)*, pp. 452-457, 2018, https://doi.org/10.1109/ICSTCC.2018.8540652.

[61] Z. Wu, G. Shi, D. Li, Y. Liu, Y. Chen, "Active Disturbance Rejection Control Design for High-Order Integral Systems," *ISA Transactions*, vol. 125, pp. 560-570, 2022, https://doi.org/10.1016/j.isatra.2021.06.038.

[62] L. Zhao, X. Liu, T. Wang, B. Liu, "A Reduced-Order Extended State Observer-Based Trajectory Tracking Control for One-Degree-of-Freedom Pneumatic Manipulator," *Advances in Mechanical Engineering*, vol. 10, no. 4, 2018, https://doi.org/10.1177/1687814018767289.

[63] Z. G. Liu, and Y. G. Jiang, "Design of a Modified Tracking Differentiator," *World Journal of Engineering and Technology*, vol. 5, no. 4, pp. 668-674, 2017, https://doi.org/10.4236/wjet.2017.54055.

[64] W. Wang and Z. Gao, "A Comparison Study of Advanced State Observer Design Techniques," *Proceedings of the 2003 American Control Conference, 2003*, vol. 6, pp. 4754-4759, 2003, https://doi.org/10.1109/ACC.2003.1242474.

[65] R. A. Kadhim, M. Q. Kadhim, H. Al-Khazraji, and A. J. Humaidi, "Bee Algorithm Based Control Design for Two-Links Robot Arm Systems," *IIUM Engineering Journal*, vol. 25, no. 2, pp. 367-380, 2024, https://doi.org/10.31436/iiumej.v25i2.3188.

[66] A. Ma'Bdeh, N. Tawalbeh and R. El-Khazali, "Sensorless Speed Control of a PMSM Using Fractional-Order Extended State Observer," *2023 International Conference on Fractional Differentiation and Its Applications (ICFDA)*, pp. 1-5, 2023, https://doi.org/10.1109/ICFDA58234.2023.10153300.

[67] A. K. Ahmed and H. Al-Khazraji, "Optimal Control Design for Propeller Pendulum Systems Using Gorilla Troops Optimization," *Journal Européen des Systèmes Automatisés*, vol. 56, no. 4, pp. 575-582, 2023, https://doi.org/10.18280/jesa.560407.

[68] Z. N. Mahmood, H. Al-Khazraji and S. M. Mahdi, "PID-Based Enhanced Flower Pollination Algorithm Controller for Drilling Process in a Composite Material," *A Composite Material. Annales de Chimie - Science des Matériaux*, vol. 47, no. 2, pp. 91-96, 2023, https://doi.org/10.18280/acsm.470205.

[69] M. A. AL-Ali, O. F. Lutfy and H. Al-Khazraj, "Comparative Study of Various Controllers Improved by Swarm Optimization for Nonlinear Active Suspension Systems with Actuator Saturation," *International Journal of Intelligent Engineering & Systems*, vol. 17, no. 4, pp. 870-881, 2024, https://doi.org/10.22266/ijies2024.0831.66.

[70] A. S. Aljuboury, A. H. Hameed, A. R. Ajel, A. J. Humaidi, A. Alkhayyat, A. K. A. Mhdawi, "Robust Adaptive Control of Knee Exoskeleton-Assistant System Based on Nonlinear Disturbance Observer," *Actuators*, vol. 11, no. 3, p. 78, 2022, https://doi.org/10.3390/act11030078.